AIAA JOURNAL
Vol. 48, No. 9, September 2010

Elastic–Plastic Analysis by Integrated Local Petrov–Galerkin Sinc Method

Wesley C. H. Slemp,* Sameer B. Mulani,† and Rakesh K. Kapania‡
Virginia Polytechnic Institute and State University, Blacksburg, Virginia 24060

DOI: 10.2514/1.J050281

Elastic and elastic–plastic analyses of tensioned panels with an elliptical center notch are performed using the integrated local Petrov–Galerkin sinc method. The method is extended for analysis of boundary-value problems for nonlinear materials. The integrated local Petrov–Galerkin sinc method is used to obtain stress concentrations and stress intensities, using the *J* integral for both elastic and elastic–plastic plane-stress panels. The material is assumed to behave in a bilinear manner with kinematic hardening. The results are compared with the analytic solution for an infinite elastic panel in tension and with a finite-element solution for the panel with material nonlinearity. Good correlation is seen with stress concentration; although, the method tends to overestimate the stress concentrations. The nonlinear results compare well with the finite-element results. The accuracy deteriorates as the plastic zone propagates into areas less densely populated by the sinc points. For the elastic–plastic material, the *J* integral was estimated within 5% of the finite-element result, using the integrated local Petrov–Galerkin sinc method.

Nomenclature

$\mathbf{A}$, $\mathbf{A}_\xi$, $\mathbf{A}_\eta$, $\mathbf{A}_{x_1}$, $\mathbf{A}_{x_2}$	=	matrices defining the basis function
a, r_1, r_2	=	domain dimensions
C_{ijkl}, C_{ij}	=	plane-stress reduced stiffness tensor expressed by fourth-order tensor and by the Voigt notation, respectively
$\mathbf{F}$, $\mathbf{f}$	=	force vector
h	=	sinc mesh size
J	=	J integral, N/m
$\mathbf{K}$	=	stiffness matrix
N	=	sinc discretization parameter
n	=	number of sinc points along each computational axis $n = 2N + 1$
$N_i(\xi, \eta)$	=	Lagrange interpolation polynomial
n_i	=	tensor of the normal vector
$\mathbf{P}_i$	=	matrix of boundary-condition penalty terms
p_i	=	traction tensor, MPa
$\mathbf{Q}$, $\mathbf{R}$	=	QR factorization of the stiffness matrix
$\mathbf{U}_i$, $\mathbf{u}$	=	unknown vectors
u_i	=	displacement tensor, m
W^I	=	weight function of the Ith subdomain
x_1, x_2	=	orthogonal coordinate basis of the physical domain, m
β	=	penalty parameter
$\Delta(\bullet)$	=	increment of respective term
ϵ_{ij}, ϵ^p_{ij}	=	infinitesimal strain tensor and plastic strain tensor
Γ, Γ_i	=	boundary and portions of the boundary of the domain Ω
ξ, η	=	orthogonal coordinate basis of computational domain
σ_{ij}	=	Cauchy stress tensor, MPa
$\phi(t)$, $\psi(\tau)$	=	mapping functions between t and τ domains
Ω	=	domain of boundary-value problem in physical domain
$(\bullet)_{,xy}$	=	partial differentiation with respect to x and y, $\partial^2(\bullet)/(\partial x \partial y)$
$(\bullet)^I$	=	quantity from the Ith weight function of compact support
${}^{(i)}(\bullet)$, ${}^{(ii)}(\bullet)$	=	quantity from the subdomain i and ii, respectively
${}^{t}(\bullet)^{(i)}$	=	quantity from the ith iteration of the load increment t

Received 8 October 2009; accepted for publication 6 January 2010.

*National Defense Science and Engineering Graduate Research Fellow, Aerospace and Ocean Engineering, Sensors and Structural Health Monitoring Group. Student Member AIAA.

†Post Doctoral Fellow, Aerospace and Ocean Engineering. Member AIAA.

‡Mitchell Professor, Aerospace and Ocean Engineering, Sensors and Structural Health Monitoring Group. Associate Fellow AIAA.

I. Introduction

STRESS analysis of notched and cracked aircraft components is an important part of understanding the fatigue-crack growth process. In the past, stable crack growth in metallic materials under mode I loading has been extensively studied, using elastic–plastic finite-element analysis (FEA) [1]. Efficient techniques have been developed to predict unstable crack growth. Fracture criteria include crack-tip stress or strain intensity factors, crack-tip-opening displacement or angle, crack-tip force, energy-release rates, J integral, and the tearing modulus. The present study focuses on the evaluation of J integral for panels with elastic–plastic materials.

The J integral was proposed by Rice in 1968 as a way to calculate the strain energy-release rate in a material [2]. The J integral is particularly useful when there is a large amount of plasticity [3]. Testing procedures for determining the fracture toughness of metallic materials using the J-integral method are prescribed according to the American Society for Testing and Materials standard E1820. The use of J integral allows the testing of a small specimen (outside the limits of linearly elastic fracture mechanics) to obtain the critical, mode I fracture energy J_{I_c}. While the J integral is typically applied to line cracks, its application to rounded and V-shaped notches was proposed by Livieri [4,5] and Berto and Lazzarin [6].

For elastic–plastic problems with proportional loading or approximately proportional loading, the path independence of the J integral still holds [7]. Furthermore, its comparison with the known critical value predicts an unstable brittle crack growth quite well [8]. However, for nonproportional loading, the J integral is path-dependent [9]. The J integral is based on the deformation theory of plasticity and holds for nonlinear elastic materials. The path independence vanishes when crack growth occurs, as most engineering materials unload drastically. Recently, the near-tip J integral was

shown to be the "scalar driving force at the crack tip even in incrementally elastic–plastic materials, based on the second law of thermodynamics" by Simha et al. [9].

Meshless methods are often advantageous over finite-element methods (FEMs), in that they possess a higher degree of continuity in the solution field. For elastic–plastic materials, this continuity of higher-order derivatives is advantageous in areas apart from the elastic–plastic boundary. Discontinuities in the derivative of the strain field across elastic–plastic boundaries, however, are physical. Therefore, the application of highly continuous methods for elastic–plastic problems should be considered carefully.

Gu et al. [10] studied material nonlinearity, using the local radial point interpolation method, a meshless local Petrov–Galerkin method (MLPG) with the radial basis function. The paper examined a constant tension specimen, a pressurized thick-walled cylinder, and a V-notched plate. In each example, the method performs quite well when compared with the FEM. Ma et al. [11] studied the use of the meshless integral method for simple elastic–plastic plane-stress and plane-strain problems. A rectangular panel under constant tension and constant shear, a finite plate with a circular hole, and a pressurized thick-walled cylinder were all solved by the meshless integral method.

In impact analysis, meshless methods have been suggested and implemented by many authors, because there is no need to remesh when failures and shear bands occur. Zhang and Chen [12] used the moving least-squares approximation in the element-free Galerkin formulation to study high-velocity impact of an elastic–plastic plate. Zhang and Chen noted that one drawback of the method is that it needs a large number of particles for accurate results for the dynamic fracture study.

The integrated local Petrov–Galerkin sinc method (ILPGSM) was recently proposed by Slemp et al. [13,14] as a weak-form-based implementation of the basis function from the sinc method, based on interpolation of the highest derivative (SIHD) [15–17]. The method was shown to generally perform better than SIHD, a collocation-based or strong-form-based approach. Furthermore, the method was shown to perform exceptionally well in the presence of an edge singularity and is much easier to implement on arbitrary, non-rectangular domains than the SIHD method. Therefore, the ILPGSM seems to be a good candidate for handling problems with a highly elliptical notch.

The remainder of this paper is arranged as follows. The most pertinent details of the ILPGSM are reviewed. The domain decomposition and iterative solution approaches are detailed. The numerical results for infinite elastic plane-stress panels with elliptical center notches are presented, with results including the J integral. Comparison is made with the analytic solution for the infinite elastic panel with an elliptical center notch. Numerical results for an elastic–plastic panel with bilinear material behavior and kinematic hardening are presented and compared with similar results from the FEM. The paper concludes with a brief summary and concluding remarks.

II. Integrated Local Petrov–Galerkin Sinc Method

The ILPGSM approach was used to analyze the two-dimensional boundary-value problem for plane-stress deformation of elastic and elastic–plastic panels with center notches to demonstrate its effectiveness for nonrectangular domains and material nonlinearity. For details regarding the ILPGSM method, please refer to Slemp et al. [13,14]. Only the most pertinent details are reviewed next, with emphasis given to extending the method for nonlinear incremental problems.

Consider a second-order two-dimensional boundary-value problem on the rectangular domain:

$$(\xi, \eta) \in \{\xi_{-N} \le \xi \le \xi_N \cup \eta_{-N} \le \eta \le \eta_N\}$$

where the boundaries ξ_{-N}, ξ_N, η_{-N}, and η_N are the limits of sinc points prescribed by the double-exponential transformation [13,14]. Then, assuming $f_{,\xi\xi\eta\eta}(\xi, \eta) = \partial^4 f/(\partial\xi^2\partial\eta^2)$ is known at the sinc points given by the double-exponential transformation, it may be approximated by a scalar product of sinc series interpolation along each dimension. Applying numerical indefinite integration by the double-exponential transformation, the lower derivatives and unknown function may be approximated by

$$\begin{aligned} f_{,\xi}(\xi, \eta) = &\sum_{i=-N}^{N}\sum_{j=-N}^{N} T_2(\xi, i)T_3(\eta, j)f_{,\xi\xi\eta\eta}(\xi_i, \eta_j) \\ &+ \sum_{j=-N}^{N} C_1(\eta_j)T_3(\eta, j) \\ &+ \sum_{i=-N}^{N}[C_2(\xi_i)T_2(\xi, i)\eta + C_4(\xi_i)T_2(\xi, i)] + C_5\eta + C_6 \end{aligned}$$

$$\begin{aligned} f_{,\eta}(\xi, \eta) = &\sum_{i=-N}^{N}\sum_{j=-N}^{N} T_3(\xi, i)T_2(\eta, j)f_{,\xi\xi\eta\eta}(\xi_i, \eta_j) \\ &+ \sum_{i=-N}^{N} C_2(\xi_i)T_3(\xi, i) \\ &+ \sum_{j=-N}^{N}[C_1(\eta_j)T_2(\eta, j)\xi + C_3(\eta_j)T_2(\eta, j)] + C_5\xi + C_7 \end{aligned}$$

$$\begin{aligned} f(\xi, \eta) = &\sum_{i=-N}^{N}\sum_{j=-N}^{N} T_3(\xi, i)T_3(\eta, j)f_{,\xi\xi\eta\eta}(\xi_i, \eta_j) \\ &+ \sum_{i=-N}^{N}[C_1(\eta_j)T_3(\eta, j)\xi + C_3(\eta_j)T_3(\eta, j)] \\ &+ \sum_{i=-N}^{N}[C_2(\xi_i)T_3(\xi, i)\eta + C_4(\xi_i)T_3(\xi, i)] \\ &+ C_5\xi\eta + C_6\xi + C_7\eta + C_8 \end{aligned}$$

where

$$T_1(\xi, j) = \operatorname{sinc}\left(\frac{\phi(\xi)}{h} - j\right) \tag{1}$$

$$T_2(\xi, j) = h\psi'(jh)\left[\frac{1}{2} + \frac{1}{\pi}\operatorname{Si}\left(\frac{\pi\phi(\xi)}{h} - \pi j\right)\right] \tag{2}$$

$$\begin{aligned} T_3(\xi, j) = &\sum_{i=-N}^{N} h^2\psi'(ih)\psi'(jh)\left[\frac{1}{2} + \frac{1}{\pi}\operatorname{Si}\left(\frac{\pi\phi(\xi)}{h} - \pi i\right)\right] \\ &\times \left\{\frac{1}{2} + \frac{1}{\pi}\operatorname{Si}[\pi(i - j)]\right\} \end{aligned} \tag{3}$$

h is the mesh size, $\operatorname{Si}(x)$ is the sine-integral function, and ϕ is the double-exponential transformation [13–17]. Note that ψ is the inverse transformation (see Slemp et al. [13,14] for the details). For the present study, the sine-integral function was evaluated by the approach described by MacLeod [18]. The unknowns are $f_{,\xi\xi\eta\eta}(\xi_i, \eta_j)$, $C_1(\eta_i)$, $C_2(\xi_i)$, $C_3(\eta_i)$, $C_4(\xi_i)$, and C_α, where the subscripts are defined by $\{i, j\} = \{-N, -N + 1, \ldots, N\}$, and $\alpha = \{5, 6, 7, 8\}$. There are $n = 2N + 1$ sinc points.

To write the basis functions in matrix form, the global unknown vector,

$$\mathbf{u} = \{\mathbf{f}_{,\xi\xi\eta\eta}, \mathbf{C}_1, \mathbf{C}_2, \mathbf{C}_3, \mathbf{C}_4, C_5, C_6, C_7, C_8\}^T$$

is introduced, where

$$\mathbf{C}_1 = \{C_1(\xi_{-N}), C_1(\xi_{-N+1}), \ldots, C_1(\xi_N)\}$$

and with similar definitions for $\mathbf{C}_2$, $\mathbf{C}_3$, and $\mathbf{C}_4$, and with

$$\mathbf{f}_{,\xi\xi\eta\eta} = \{f_{,\xi\xi\eta\eta}(\xi_{-N}, \eta_{-N}), f_{,\xi\xi\eta\eta}(\xi_{-N+1}, \eta_{-N}), \ldots, f_{,\xi\xi\eta\eta}(\xi_N, \eta_{-N}), \times f_{,\xi\xi\eta\eta}(\xi_{-N}, \eta_{-N+1}), \ldots, f_{,\xi\xi\eta\eta}(\xi_N, \eta_N)\}$$

The basis function is written in matrix form:

$$f_{,\xi}(\xi,\eta) = \mathbf{A}_\xi(\xi,\eta)\mathbf{u}; \quad f_{,\eta}(\xi,\eta) = \mathbf{A}_\eta(\xi,\eta)\mathbf{u}; \quad f(\xi,\eta) = \mathbf{B}(\xi,\eta)\mathbf{u} \tag{4}$$

where $\mathbf{A}_\xi$,$\mathbf{A}_\eta$, and $\mathbf{B}$ were defined in Slemp et al. [13,14].

A. Domain Decomposition and Mapping

The present analysis considers domains with elliptic and circular holes. Thus, the rectangular computational domain (ξ, η) must be transformed to the physical domain. The simplest method for domain transformation is to follow the methodology of isoparametric elements in a quadrilateral finite element. While using the displacement shape functions to describe the shape of element boundaries is not the intent, using the Lagrange interpolation polynomials with a discrete number of nodes provides a good means to approximately represent the geometry. Consider Fig. 1. The figure indicates a nine-node subdomain in the computational domain (ξ, η) and physical domain. Note that the term node is used to describe a point of exact geometric match between the physical domain and the computational domain. These points are not related to the sinc points of the ILPGSM method. The mapping between the two domains is given by

$$x_1 = N_i(\xi,\eta)x_{1i}; \qquad x_2 = N_i(\xi,\eta)x_{2i} \tag{5}$$

where $N_i(\xi, \eta)$ are the Lagrange shape functions [19].

Consider a quarter of a symmetric panel with a center elliptic notch, as shown in Fig. 2, with dimensions, loads, and boundary conditions indicated. Because the domain has five distinct edges, a single mapping between computational and physical domains would not be unique; however, using two subdomains makes the mapping quite simple (see Fig. 3). For the present study, the domains are divided along the line $(x_1 = x_2)$. It should be noted that additional benefit from using additional subdomains would be marginal. While this has been neither rigidly proved nor numerically verified, the additional constants of integration and the necessity of a convergent sinc series imply a minimal number of subdomains are desired.

To express derivatives with respect to the physical domain coordinates x_1 and x_2, the domain mapping is differentiated, resulting in the following relations:

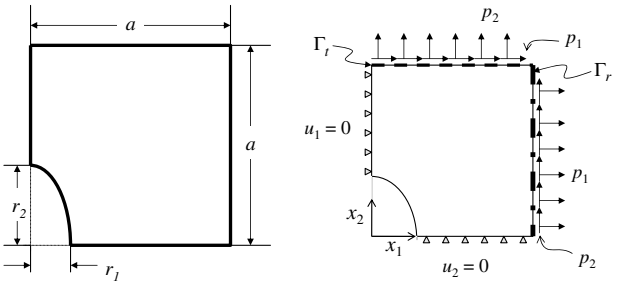

a) Dimensions **b) Boundary conditions**

Fig. 2 Notched plane-stress members: dimensions and loads.

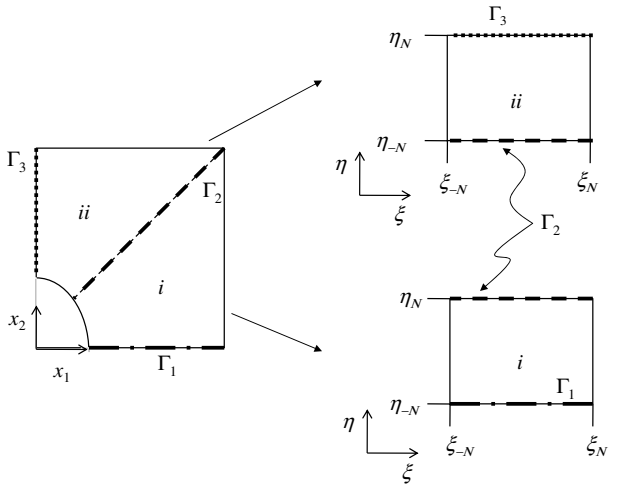

Fig. 3 Domain decomposition and transformation onto two rectangular domains with boundary contours Γ_1, Γ_2, and Γ_3 indicated.

$$\frac{\partial\xi}{\partial x_1} = \frac{1}{|J|}\frac{\partial N_i}{\partial\eta}x_{2i}; \qquad \frac{\partial\xi}{\partial x_2} = -\frac{1}{|J|}\frac{\partial N_i}{\partial\eta}x_{1i};$$
$$\frac{\partial\eta}{\partial x_1} = -\frac{1}{|J|}\frac{\partial N_i}{\partial\xi}x_{2i}; \qquad \frac{\partial\eta}{\partial x_2} = \frac{1}{|J|}\frac{\partial N_i}{\partial\xi}x_{1i}; \tag{6}$$
$$|J| = \left(\frac{\partial N_i}{\partial\xi}x_{1i}\frac{\partial N_j}{\partial\eta}x_{2j} - \frac{\partial N_i}{\partial\eta}x_{1i}\frac{\partial N_j}{\partial\xi}x_{2j}\right)$$

with repeated index implying summation. Thus, derivatives in the physical domain can be expressed through the basis function by

$$\frac{\partial f}{\partial x_1} = \frac{\partial\xi}{\partial x_1}\mathbf{A}_\xi\mathbf{u} + \frac{\partial\eta}{\partial x_1}\mathbf{A}_\eta\mathbf{u} = \mathbf{A}_{x_1}(\xi,\eta)\mathbf{u};$$
$$\frac{\partial f}{\partial x_2} = \frac{\partial\xi}{\partial x_2}\mathbf{A}_\xi\mathbf{u} + \frac{\partial\eta}{\partial x_2}\mathbf{A}_\eta\mathbf{u} = \mathbf{A}_{x_2}(\xi,\eta)\mathbf{u}; \qquad f(\xi,\eta) = \mathbf{B}(\xi,\eta)\mathbf{u} \tag{7}$$

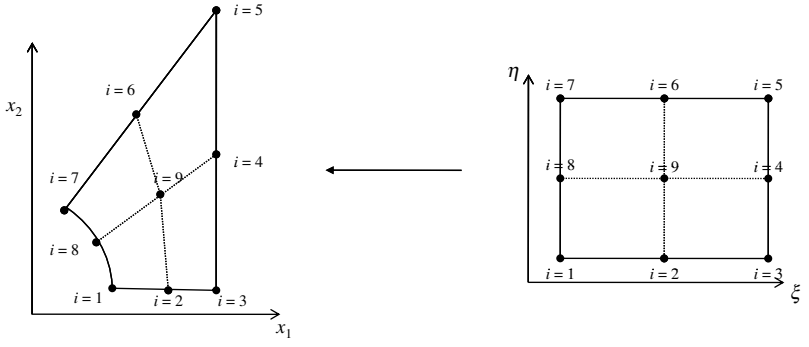

Fig. 1 Domain transformation using Lagrange interpolation polynomials

B. Incremental-Iterative Approach

For an inelastic plane-stress problem, the boundary-value problem is derived from the principle of virtual work for the geometry, shown in Fig. 2, with loading on the top and right edges. The balance of internal and external virtual work can be written as

$$\int_\Omega {}^{t+\Delta t}\sigma_{ij}\delta^{t+\Delta t}\epsilon_{ij}\,\mathrm{d}\Omega = \int_{\Gamma_r} {}^{t+\Delta t}p_i\delta^{t+\Delta t}u_i\,\mathrm{d}\Gamma_r + \int_{\Gamma_t} {}^{t+\Delta t}p_j\delta^{t+\Delta t}u_j\,\mathrm{d}\Gamma_t \tag{8}$$

where p_i is the components of applied traction to the top edge Γ_t and the right edge Γ_r, as indicated in Fig. 2. Note that p_1 is an applied normal stress σ_{11}, and p_2 is an applied shear σ_{12} on the edge Γ_r; p_1 is an applied shear σ_{12}, and p_2 is an applied normal σ_{22} on the edge Γ_t. To linearize the variational statement, the stresses, strains, and displacements are expressed by an increment from the previous load step t (the present study considers infinitesimal strains):

$$\int_\Omega ({}^t\sigma_{ij} + \Delta\sigma_{ij})\delta\Delta\epsilon_{ij}\,\mathrm{d}\Omega = \int_{\Gamma_r} {}^{t+\Delta t}p_i\delta\Delta u_i\,\mathrm{d}\Gamma_r + \int_{\Gamma_t} {}^{t+\Delta t}p_j\delta\Delta u_j\,\mathrm{d}\Gamma_t \tag{9}$$

Note that variations of stress, strain, and displacement at load step t are zero, because equilibrium is satisfied at that time step. By expressing the strain increments in terms of the displacements, the variational statement is written as

$$\int_\Omega [({}^t\sigma_{11} + \Delta\sigma_{11})\delta\Delta u_{1,1} + ({}^t\sigma_{22} + \Delta\sigma_{22})\delta\Delta u_{2,2} + ({}^t\sigma_{12} + \Delta\sigma_{12})(\delta\Delta u_{1,2} + \delta\Delta u_{2,1})]\,\mathrm{d}\Omega = \int_{\Gamma_r} {}^{t+\Delta t}p_i\delta\Delta u_i\,\mathrm{d}\Gamma_r + \int_{\Gamma_t} {}^{t+\Delta t}p_j\delta\Delta u_j\,\mathrm{d}\Gamma_t \tag{10}$$

Because the variations are arbitrary, equilibrium is satisfied by letting $\delta u_1 = 0$ with $\delta u_2 = w_2$ and $\delta u_2 = 0$ with $\delta u_1 = w_1$, where w_1 and w_2 are arbitrary. For the present study, we choose $w_1 = w_2 = W^I$, where W^I is a weight function of compact for the Ith subdomain. Therefore, the equilibrium equations may be uncoupled to yield

$$\int_\Omega [({}^t\sigma_{11} + \Delta\sigma_{11})W^I_{,1} + ({}^t\sigma_{12} + \Delta\sigma_{12})W^I_{,2}]\,\mathrm{d}\Omega = \int_{\Gamma_r}^{t+\Delta t} p_1 W^I\,\mathrm{d}\Gamma_r + \int_{\Gamma_t}^{t+\Delta t} p_1 W^I\,\mathrm{d}\Gamma_t;$$
$$\int_\Omega [({}^t\sigma_{22} + \Delta\sigma_{22})W^I_{,2} + ({}^t\sigma_{12} + \Delta\sigma_{12})W^I_{,1}]\,\mathrm{d}\Omega = \int_{\Gamma_r}^{t+\Delta t} p_2 W^I\,\mathrm{d}\Gamma_r + \int_{\Gamma_t}^{t+\Delta t} p_2 W^I\,\mathrm{d}\Gamma_t \tag{11}$$

The increment on stress is expressed in terms of the increment of strain and the plane-stress reduced, tangential stiffness matrix ${}^t\bar{C}_{ijkl}$. Next, the increment of strains is expressed in terms of derivatives of the increment of displacements. The Voigt notation was adopted to reduce the fourth-rank stiffness tensor into a second rank tensor, and the isotopicity was explicitly implemented ($\bar{C}_{1111} = \bar{C}_{11}$, $\bar{C}_{2222} = \bar{C}_{22}$, $\bar{C}_{1122} = \bar{C}_{2211} = \bar{C}_{12} = \bar{C}_{21}$, $\bar{C}_{1112} = \bar{C}_{1121} = \bar{C}_{1211} = \bar{C}_{2111} = 0$, $\bar{C}_{2212} = \bar{C}_{2221} = \bar{C}_{1222} = \bar{C}_{2122} = 0$, and $\bar{C}_{1212} = \bar{C}_{2121} = \bar{C}_{1221} = \bar{C}_{2112} = \bar{C}_{66}$). Accordingly, the equilibrium equation is expressed in terms of the previous load step, stiffnesses, weight functions, and increments on the derivatives of displacements:

$$\int_\Omega (W^I_{,1}\bar{C}_{11}\Delta u_{1,1} + W^I_{,2}\bar{C}_{66}\Delta u_{1,2})\,\mathrm{d}\Omega + \int_\Omega (W^I_{,1}\bar{C}_{12}\Delta u_{2,2} + W^I_{,2}\bar{C}_{66}\Delta u_{2,1})\,\mathrm{d}\Omega = \int_{\Gamma_r} {}^{t+\Delta t}p_1 W^I\,\mathrm{d}\Gamma_r + \int_{\Gamma_t} {}^{t+\Delta t}p_1 W^I\Gamma_t - \int_\Omega (W^I_{,1}{}^t\sigma_{11} + W^I_{,2}{}^t\sigma_{12})\,\mathrm{d}\Omega \tag{12}$$

$$\int_\Omega (W^I_{,1}\bar{C}_{66}\Delta u_{1,2} + W^I_{,2}\bar{C}_{12}\Delta u_{1,1})\,\mathrm{d}\Omega + \int_\Omega (W^I_{,1}\bar{C}_{66}\Delta u_{2,1} + W^I_{,2}\bar{C}_{22}\Delta u_{2,2})\,\mathrm{d}\Omega = \int_{\Gamma_r} {}^{t+\Delta t}p_2 W^I\,\mathrm{d}\Gamma_r + \int_{\Gamma_t} {}^{t+\Delta t}p_2 W^I\Gamma_t - \int_\Omega (W^I_{,1}{}^t\sigma_{12} + W^I_{,2}{}^t\sigma_{22})\,\mathrm{d}\Omega \tag{13}$$

The basis function [Eq. (7)] was used to approximate the incremental displacements and their derivatives. Equilibrium can be expressed in matrix form by the following equations:

$$\mathbf{K}^I_{11}\Delta\mathbf{U}_1 + \mathbf{K}^I_{12}\Delta\mathbf{U}_2 = \mathbf{F}^I_1; \qquad \mathbf{K}^I_{21}\Delta\mathbf{U}_1 + \mathbf{K}^I_{22}\Delta\mathbf{U}_2 = \mathbf{F}^I_2 \tag{14}$$

where

$$\mathbf{K}^I_{11} = \int_\Omega (W^I_{,1}\bar{C}_{11}\mathbf{A}_{x_1} + W^I_{,2}\bar{C}_{66}\mathbf{A}_{x_2})\,\mathrm{d}\Omega;$$
$$\mathbf{K}^I_{12} = \int_\Omega (W^I_{,1}\bar{C}_{12}\mathbf{A}_{x_2} + W^I_{,2}\bar{C}_{66}\mathbf{A}_{x_1})\,\mathrm{d}\Omega;$$
$$\mathbf{K}^I_{21} = \int_\Omega (W^I_{,1}\bar{C}_{66}\mathbf{A}_{x_2} + W^I_{,2}\bar{C}_{12}\mathbf{A}_{x_1})\,\mathrm{d}\Omega;$$
$$\mathbf{K}^I_{22} = \int_\Omega (W^I_{,1}\bar{C}_{66}\mathbf{A}_{x_1} + W^I_{,2}\bar{C}_{22}\mathbf{A}_{x_2})\,\mathrm{d}\Omega;$$
$$\mathbf{F}^I_1 = \int_{\Gamma_r} {}^{t+\Delta t}p_1 W^I\,\mathrm{d}\Gamma_r + \int_{\Gamma_t} {}^{t+\Delta t}p_1 W^I\Gamma_t - \int_\Omega (W^I_{,1}{}^t\sigma_{11} + W^I_{,2}{}^t\sigma_{12})\,\mathrm{d}\Omega;$$
$$\mathbf{F}^I_2 = \int_{\Gamma_r} {}^{t+\Delta t}p_2 W^I\,\mathrm{d}\Gamma_r + \int_{\Gamma_t} {}^{t+\Delta t}p_2 W^I\Gamma_t - \int_\Omega (W^I_{,1}{}^t\sigma_{12} + W^I_{,2}{}^t\sigma_{22})\,\mathrm{d}\Omega \tag{15}$$

By selecting N_{int} weight functions of compact support, Eq. (14) becomes $2N_{\mathrm{int}}$ equations.

In the present study, the weight functions were chosen to have a quadratic variation over a rectangular support in the (ξ, η) domain (see Slemp et al. [13,14]). The weight functions are zero outside of this support. By Eq. (6), the derivatives of the weights with respect to the physical coordinates may be evaluated at a given (ξ, η). Therefore, the integration in Eq. (15) is well suited to be done by Gauss quadrature in the (ξ, η) domain over the support of weight function I. The approximation to $\mathbf{K}^I_{11}$ in Eq. (15) can be written as

$$\mathbf{K}^I_{11} = \sum_{i=1}^{N_{\mathrm{ipt}}}\sum_{j=1}^{N_{\mathrm{ipt}}} w(\xi_i)w(\eta_j)[W^I_{,1}(\xi_i,\eta_j)\bar{C}_{11}(\xi_i,\eta_j)\mathbf{A}_{x_1}(\xi_i,\eta_j) + W^I_{,2}(\xi_i,\eta_j)\bar{C}_{66}(\xi_i,\eta_j)\mathbf{A}_{x_2}(\xi_i,\eta_j)]|J|(\xi_i,\eta_j) \times \frac{(\xi_{\max}-\xi_{\min})(\eta_{\max}-\eta_{\min})}{4} \tag{16}$$

where $|J|$ is the Jacobian of the domain transformation given in Eq. (6) and $\xi_{\min}$, $\xi_{\max}$, $\eta_{\min}$, and $\eta_{\max}$ are the boundaries in the support of weight function I. Similarly, the contour integrals in $\mathbf{F}^I_1$ may be approximated by

$$\int_{\Gamma_r} p_1 W^I \, \mathrm{d}\Gamma_r = \sum_{j=1}^{N_{\text{ipt}}} w(\eta_j) p_1(\xi_N, \eta_j) W^I(\xi_N, \eta_j) \times \sum_{i=1}^{9} \sqrt{\left(\frac{\partial N_i}{\partial \eta} x_{1i}\right)^2 + \left(\frac{\partial N_i}{\partial \eta} x_{2i}\right)^2} \frac{\eta_{\max} - \eta_{\min}}{2};$$

$$\int_{\Gamma_t} p_1 W^I \, \mathrm{d}\Gamma_t = \sum_{i=1}^{N_{\text{ipt}}} w(\xi_i) p_1(\xi_i, \eta_N) W^I(\xi_i, \eta_N) \times \sum_{i=1}^{9} \sqrt{\left(\frac{\partial N_i}{\partial \xi} x_{1i}\right)^2 + \left(\frac{\partial N_i}{\partial \xi} x_{2i}\right)^2} \frac{\xi_{\max} - \xi_{\min}}{2} \tag{17}$$

Because the complete physical domain was divided into two subdomains, there are two sets of $2N_{\text{int}}$ equations. Let ${}^{(i)}\mathbf{K}_{kl}$ indicate the collection of row matrices, $\mathbf{K}^I_{kl}$, for all integration weights ($I = 1, 2, \ldots, N_{\text{int}}$) and for the i subdomain, as indicated in Fig. 3, and let ${}^{(ii)}\mathbf{K}_{kl}$ indicate the collection of row matrices, $\mathbf{K}^I_{kl}$, for all integration weights ($I = 1, 2, \ldots, N_{\text{int}}$) and for the ii subdomain. Then, the complete system of equations is given by

$$\begin{bmatrix} {}^{(i)}\mathbf{K}_{11} & {}^{(i)}\mathbf{K}_{12} & 0 & 0 \\ {}^{(i)}\mathbf{K}_{21} & {}^{(i)}\mathbf{K}_{22} & 0 & 0 \\ 0 & 0 & {}^{(ii)}\mathbf{K}_{11} & {}^{(ii)}\mathbf{K}_{12} \\ 0 & 0 & {}^{(ii)}\mathbf{K}_{21} & {}^{(ii)}\mathbf{K}_{22} \end{bmatrix} \begin{Bmatrix} {}^{(i)}\Delta\mathbf{U}_1 \\ {}^{(i)}\Delta\mathbf{U}_2 \\ {}^{(ii)}\Delta\mathbf{U}_1 \\ {}^{(ii)}\Delta\mathbf{U}_2 \end{Bmatrix} = \begin{Bmatrix} {}^{(i)}\mathbf{F}_1 \\ {}^{(i)}\mathbf{F}_2 \\ {}^{(ii)}\mathbf{F}_1 \\ {}^{(ii)}\mathbf{F}_2 \end{Bmatrix} \tag{18}$$

It should be noted that, in Eq. (18), the subdomains are uncoupled and singular, because continuity between the subdomains and the essential boundary conditions has yet to be enforced. To enforce the essential boundary conditions and continuity between the two subdomains, the traditional penalty method was used. The following additional contour integrals were evaluated:

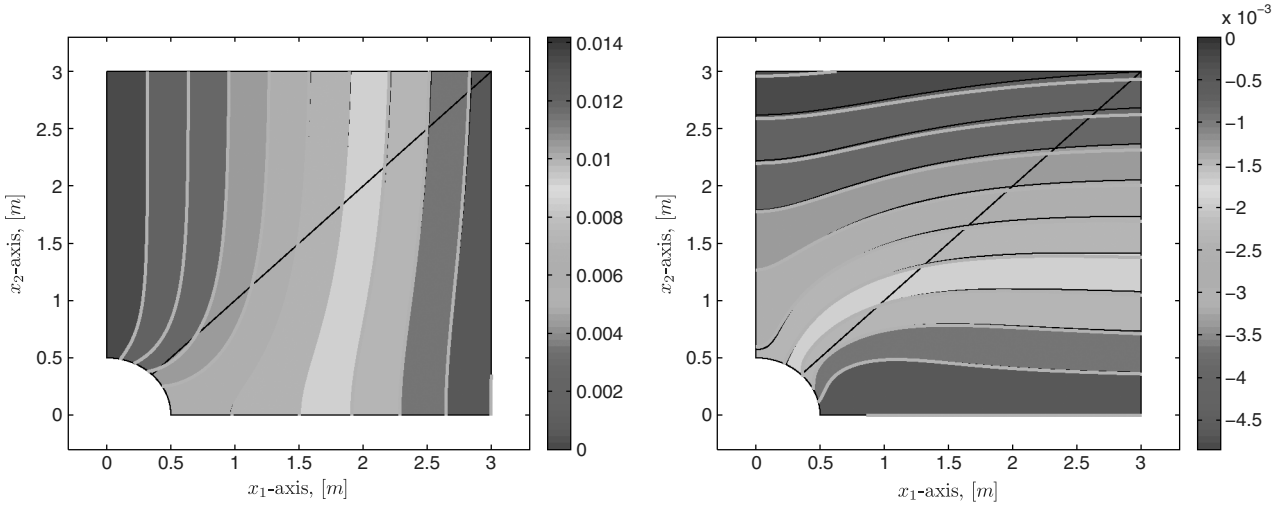

a) $10^3 \times u_1$, mm **b) $10^3 \times u_2$, mm**

Fig. 4 Displacement contours for a panel with a circular notch by ILPGSM and the analytic solution.

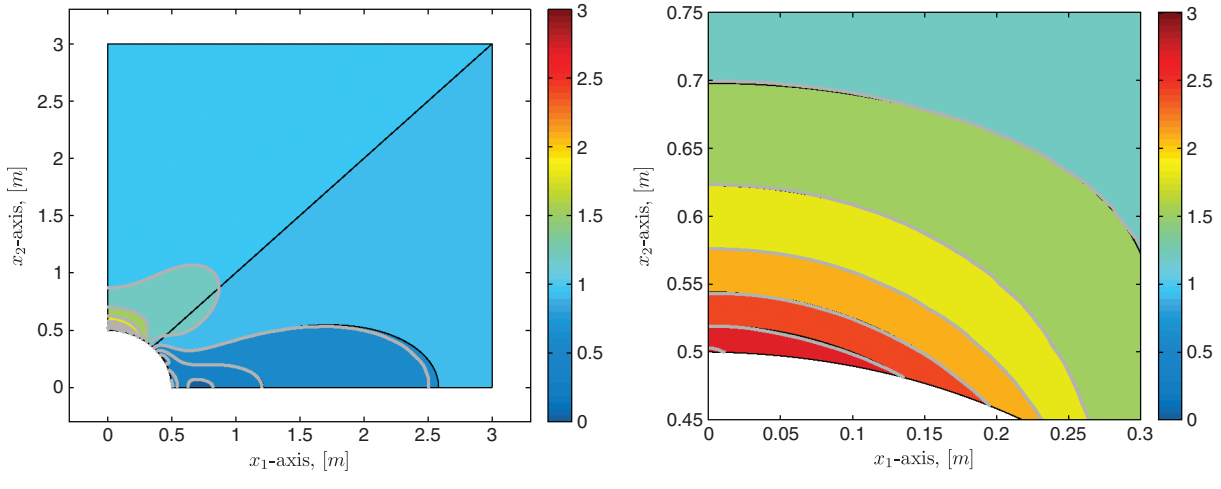

a) Complete domain **b) Near the hole**

Fig. 5 Contours of von Mises stress for a panel with a circular notch, by ILPGSM and the analytic solution.

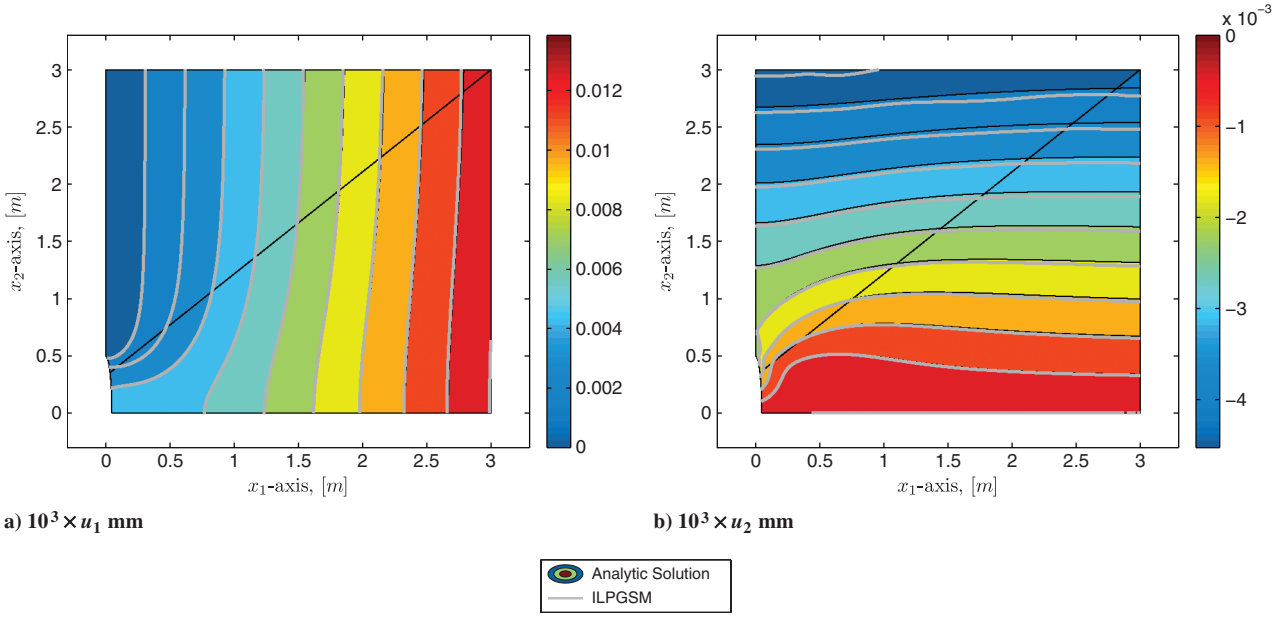

a) $10^3 \times u_1$ mm b) $10^3 \times u_2$ mm

Fig. 6 Displacement contours for a panel with an elliptical notch with an aspect ratio of $r_2/r_1 = 10$, by ILPGSM and the analytic solution.

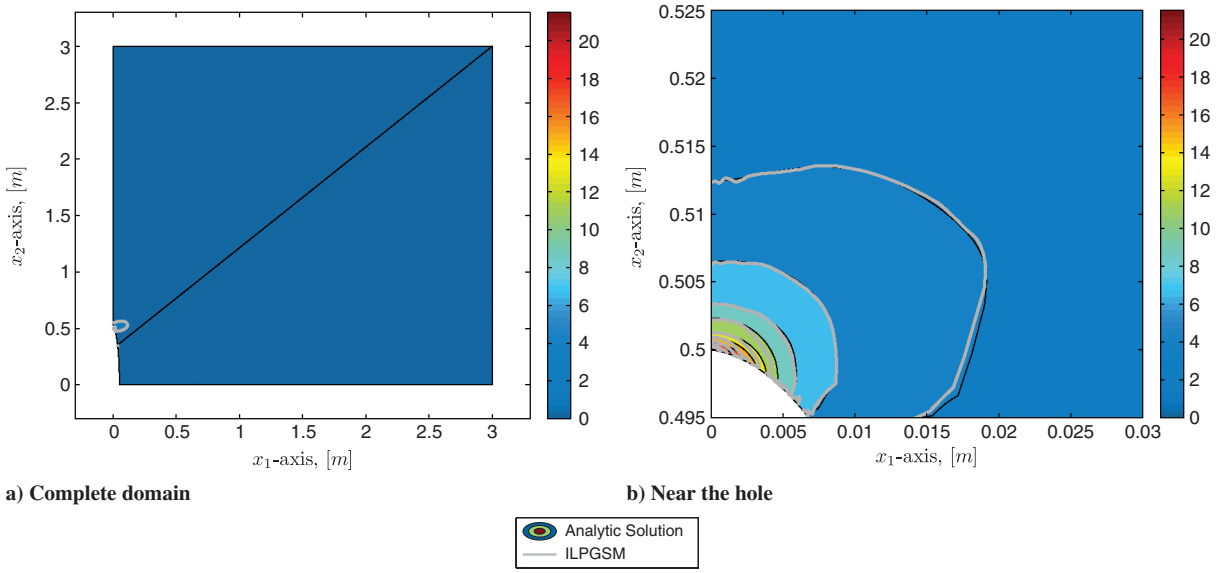

a) Complete domain b) Near the hole

Fig. 7 Contours of von Mises stress for a panel with an elliptical notch with an aspect ratio of 10, by ILPGSM and the analytic solution.

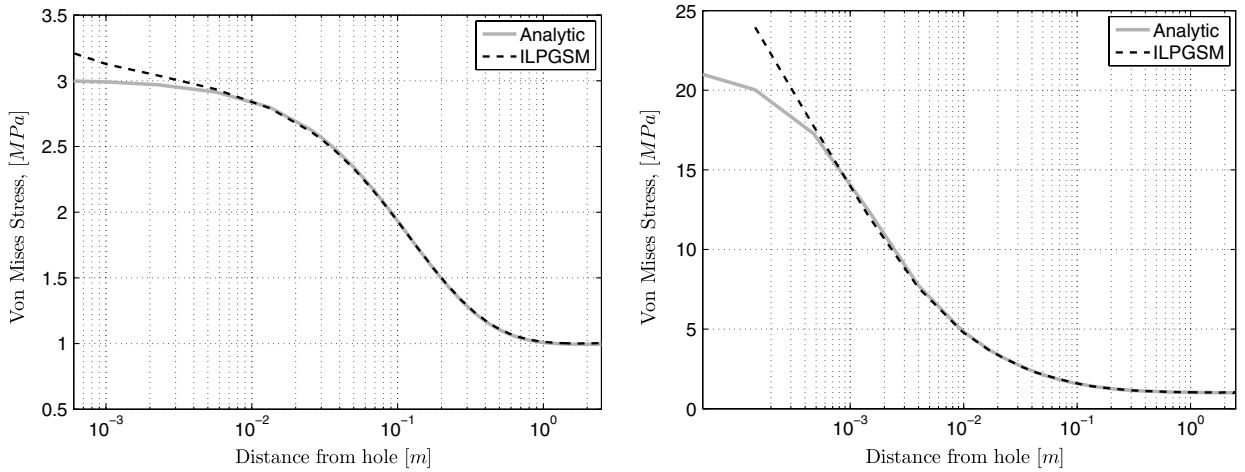

a) $r_2/r_1 = 1$ b) $r_2/r_1 = 10$

Fig. 8 Von Mises stress along $x_1 = 0$ in the vicinity of the hole.

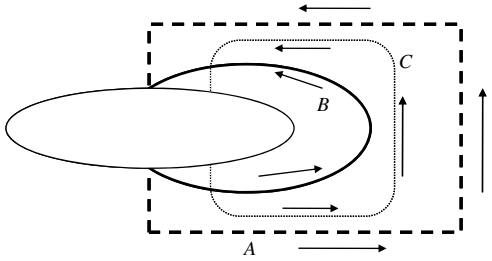

Fig. 9 Path dependence of *J* integral for elliptical hole

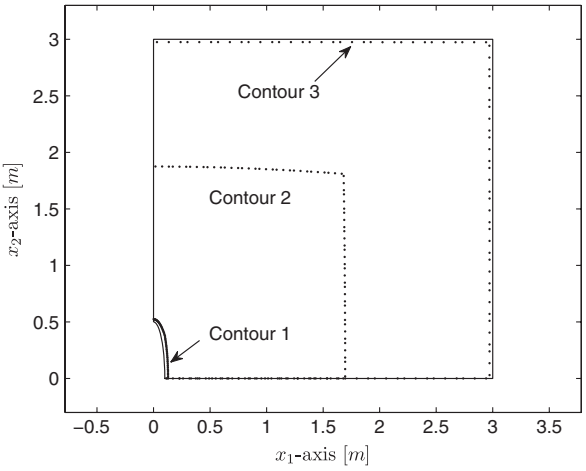

Fig. 10 Paths on which the *J* integral was computed and averaged for the elliptical notch with aspect ratio of 5.

$$
\begin{aligned}
\mathbf{P}_1 &= \beta \int_{\Gamma_1} {}^{(i)}W^{I(i)}\mathbf{B}(\xi,\eta)\,\mathrm{d}\Gamma_1;\\
\mathbf{P}_2 &= \beta \int_{\Gamma_2} {}^{(i)}W^{I(i)}\mathbf{B}(\xi,\eta)\,\mathrm{d}\Gamma_2;\\
\mathbf{P}_3 &= \beta \int_{\Gamma_2} {}^{(i)}W^{I(ii)}\mathbf{B}(\xi,\eta)\,\mathrm{d}\Gamma_2;\\
\mathbf{P}_4 &= \beta \int_{\Gamma_2} {}^{(ii)}W^{I(i)}\mathbf{B}(\xi,\eta)\,\mathrm{d}\Gamma_2;\\
\mathbf{P}_5 &= \beta \int_{\Gamma_2} {}^{(ii)}W^{I(ii)}\mathbf{B}(\xi,\eta)\,\mathrm{d}\Gamma_2;\\
\mathbf{P}_6 &= \beta \int_{\Gamma_3} {}^{(i)}W^{I(ii)}\mathbf{B}(\xi,\eta)\,\mathrm{d}\Gamma_3
\end{aligned}
\tag{19}
$$

Table 1 Elastic–plastic material properties for a typical aluminum alloy

Properties	Values
E, GPa	70
σ_y, MPa	400
ν	0.33
E_p, GPa	1.4

where the contours Γ_1, Γ_2, and Γ_3 are defined in Fig. 3, and β is a penalty parameter. Zhu and Atluri [20] suggest a range of $(10^3 - 10^7)E$ for the penalty parameter. For the present implementation, β was chosen to be $10^6 E$. These matrices can be approximated by Gauss quadrature in a similar fashion to that given in Eq. (17).

The domain is fully constrained by augmenting the system of equations in the appropriate fashion:

$$
\begin{bmatrix}
{}^{(i)}\mathbf{K}_{11}+\mathbf{P}_2 & {}^{(i)}\mathbf{K}_{12} & -\mathbf{P}_3 & 0\\
{}^{(i)}\mathbf{K}_{21} & {}^{(i)}\mathbf{K}_{22}+\mathbf{P}_1+\mathbf{P}_2 & 0 & -\mathbf{P}_3\\
-\mathbf{P}_5 & 0 & {}^{(ii)}\mathbf{K}_{11}+\mathbf{P}_4+\mathbf{P}_6 & {}^{(ii)}\mathbf{K}_{12}\\
0 & -\mathbf{P}_5 & {}^{(ii)}\mathbf{K}_{21} & {}^{(ii)}\mathbf{K}_{22}+\mathbf{P}_4
\end{bmatrix}
\times
\begin{Bmatrix}
{}^{(i)}\Delta\mathbf{U}_1\\ {}^{(i)}\Delta\mathbf{U}_2\\ {}^{(ii)}\Delta\mathbf{U}_1\\ {}^{(ii)}\Delta\mathbf{U}_2
\end{Bmatrix}
=
\begin{Bmatrix}
{}^{(i)}\mathbf{F}_1-\mathbf{P}_2^{(i)}\mathbf{U}_1+\mathbf{P}_3^{(ii)}\mathbf{U}_1\\
{}^{(i)}\mathbf{F}_2-(\mathbf{P}_1+\mathbf{P}_2)^{(i)}\mathbf{U}_2+\mathbf{P}_3^{(ii)}\mathbf{U}_2\\
{}^{(ii)}\mathbf{F}_1-(\mathbf{P}_4+\mathbf{P}_6)^{(ii)}\mathbf{U}_1+\mathbf{P}_5^{(i)}\mathbf{U}_1\\
{}^{(ii)}\mathbf{F}_2-\mathbf{P}_4^{(ii)}\mathbf{U}_2+\mathbf{P}_5^{(i)}\mathbf{U}_2
\end{Bmatrix}
\tag{20}
$$

or in a simplified form:

$$
{}^{t}\mathbf{K}^{(i)}\Delta\mathbf{u} = {}^{t}\mathbf{f}^{(i)} \tag{21}
$$

where the right superscript (i) implies the ith iteration of load step t. The global unknown vector ${}^{t}\mathbf{u}^{(i)}$ may be iterated by the Newton–Raphson method:

$$
{}^{t}\mathbf{u}^{(i)} = \Delta\mathbf{u} + {}^{t}\mathbf{u}^{(i-1)} \tag{22}
$$

Equations (21) and (22) can be repeatedly used to increment ${}^{t}\mathbf{u}$ until a convergence criteria is satisfied. However, populating and factorizing $\mathbf{K}$ for each iteration and load step would be extraordinarily expensive. Thus, the modified Newton method is employed, and $\mathbf{K}$ is only populated and factorized once:

$$
{}^{t=0}\mathbf{K}^{(i=1)}\Delta\mathbf{u} = {}^{t}\mathbf{f}^{(i)} \tag{23}
$$

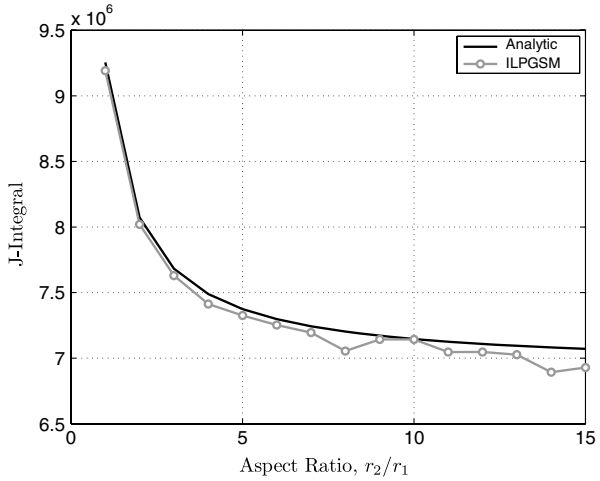

a) Comparison of J integral to analytic solution

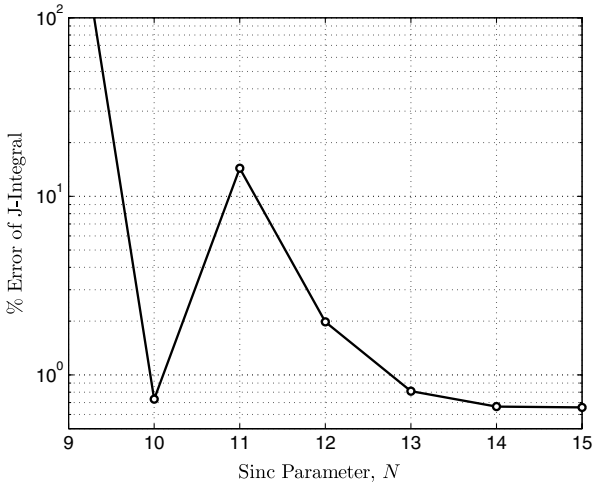

b) Convergence with Increasing N for $r_2/r_1 = 5$

Fig. 11 Comparison of *J* integral by ILPGSM with the analytic solution. *J* integral given in units of N/m.

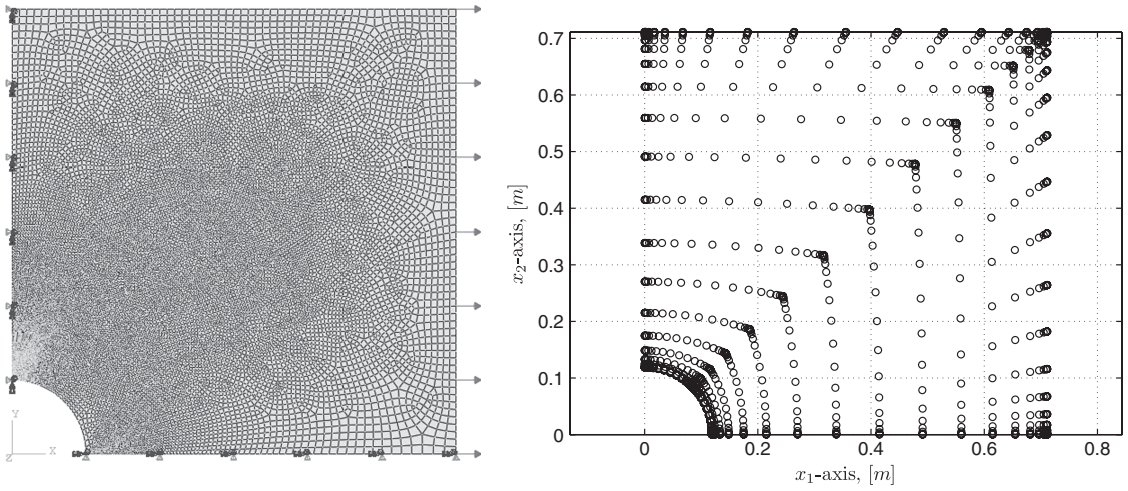

a) FEA mesh **b) ILPGSM sinc points**

Fig. 12 Converged FEA mesh and ILPGSM sinc point distribution for elastic–plastic plane-stress panel with circular notch.

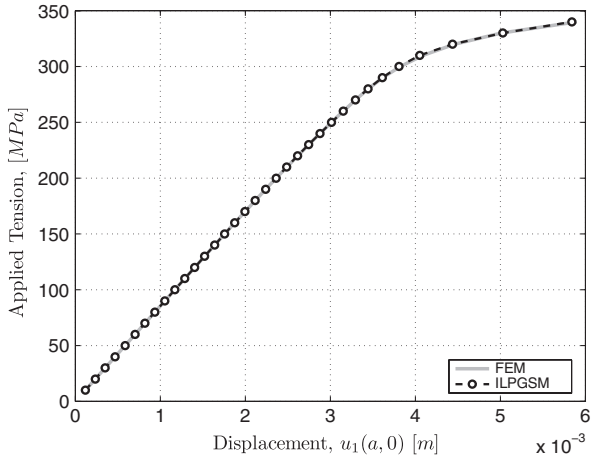

Fig. 13 Displacement of the point $(a, 0)$ versus applied tension load. The onset of plasticity occurs at about 130 MPa.

Initial analysis with the ILPGSM indicated the additional accuracy can be achieved by overdetermining the system of equations [13]. Furthermore, applying the continuity condition between the elements via the penalty method can cause ill conditioning. The advantage of overdetermining the system is that the additional information (more weight function or test equations) allows the ILPGSM to obtain a converged solution despite the conditioning. This was done by choosing more weight functions than unknowns, thus resulting in more equations. The overdetermined least-squares approach is often a standard approach with the MLPG [21]. Thus, the QR decomposition was used to factorize the stiffness matrix. That is, for $\mathbf{K}$ having dimensions $n \times m$, where $n > m$, determines matrices $\mathbf{Q}$ and $\mathbf{R}$, such that

$$\mathbf{K} = \mathbf{QR} \tag{24}$$

where $\mathbf{Q}$ is $n \times n$ matrix, and $\mathbf{R}$ is an $n \times m$ upper triangular matrix. Letting the top m rows of $\mathbf{Q}$ and $\mathbf{R}$ be $\tilde{\mathbf{Q}}$ and $\tilde{\mathbf{R}}$, respectively, then the least-squares solution to Eq. (21) is approximated by

$$\tilde{\mathbf{R}}\Delta\mathbf{u} = \tilde{\mathbf{Q}}^T({}^t\mathbf{f}_{(i)}) \tag{25}$$

Note that, because $\tilde{\mathbf{R}}$ is upper triangular, the global increment $\Delta\mathbf{u}$ is estimated without the expense of populating and factorizing $\mathbf{K}$.

III. Numerical Results for Elastic Notched Panel

For numerical evaluation, an elastic, infinite, plane-stress panel with an elliptical notch was considered. The problem was analyzed by Batra and Zhang [22] for an infinite panel with a circular hole. For the sake of comparison, material properties and dimensions were chosen to remain consistent with Batra and Zhang [22]. To that

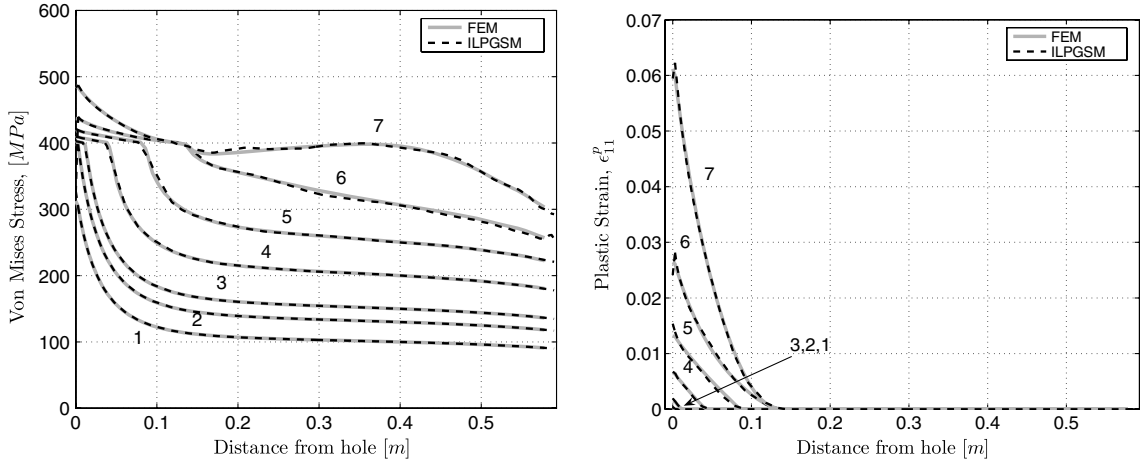

a) Von mises stress **b) Plastic strain**

Fig. 14 Von Mises stress and plastic strain for panel with circular notch. Load steps 1–100, 2–130, 3–150, 4–200, 5–250, 6–300, and 7–340 MPa.

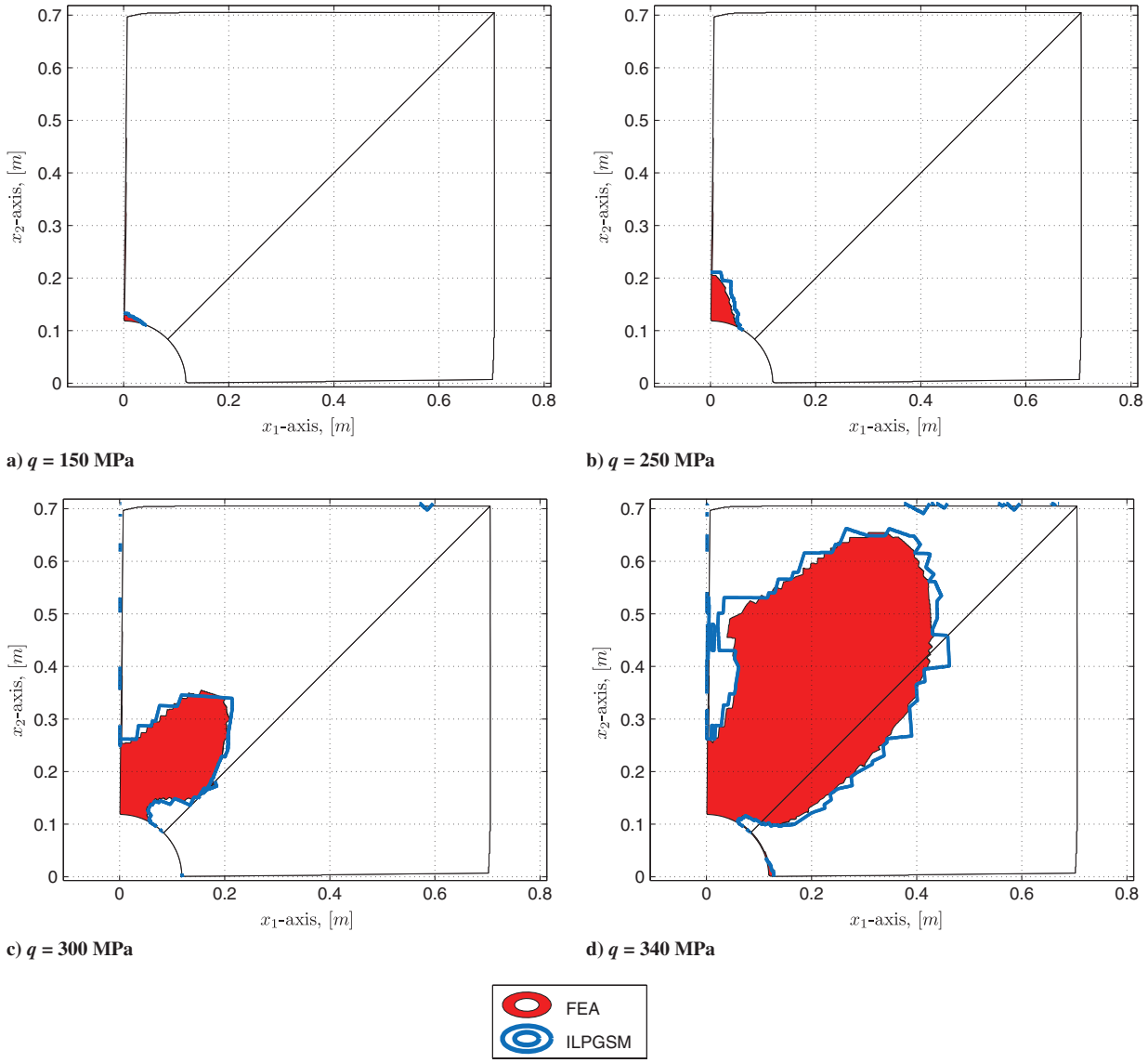

Fig. 15 Growth of plastic zone with increasing applied load by ILPGSM and FEA. The red and blue contours indicate yielded material from the FEA and ILPGSM, respectively.

regard, the semimajor axis was specified to be $r_2 = 0.5$ m and the aspect ratio r_2/r_1 varied. The following isotropic elastic material properties were chosen: $E = 226.9$ GPA, and $\nu = 0.33$. An analytic solution for the present problem is well known [23]. While the panel is infinite, only the innermost square was modeled, and the traction boundary conditions were applied from the analytic solution so that this solution remains valid. Both normal and shear traction along the top and right edges were imposed from the analytic solution [23]. Remaining consistent with Batra and Zhang [22], a square segment was modeled with $a = 3$ m, as indicated in Fig. 2.

The ILPGSM results were obtained using a sinc mesh size taken to be $h = 2/N$, which was shown to provide good convergence properties for the previous studies with integrated sinc methods [13,14]. The number of particles along each axis in the sinc approximation was chosen by setting $N = 14$; that is, $n = 29$ sinc points along each edge.

Contours of displacement are compared for the present method and the analytic solution in Fig. 4 for a circular hole ($a/b = 1$). The contours of the ILPGSM results are virtually indistinguishable from the analytic solution, indicating the ILPGSM solution provides a very accurate numerical solution for the displacements in the present problem.

Contours of von Mises stress were plotted in Fig. 5 for the complete domain and zoomed in near the hole. Note that the contours are almost indistinguishable from the analytic solution. There is some error in the solution near the line $2 \le x_1 \le 2.5$, $x_2 = 0$. However, the degree to which the stress concentration is approximated in the vicinity of the notch is quite excellent.

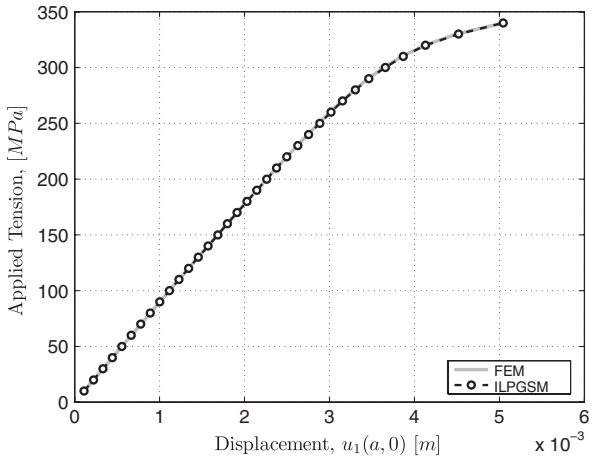

Fig. 16 Displacement of the point $(a, 0)$ versus applied tension load. The onset of plasticity occurs at about 36 MPa.

Similar results were obtained for an elliptical hole with an aspect ratio of 10 ($r_2/r_1 = 10$). The contours of displacement are plotted in Fig. 6, and contours of von Mises stress are plotted in Fig. 7. For the severe notch, the ILPGSM still performs extremely well. The ILPGSM and the analytic solutions are significantly distinguishable only in the vicinity of the $x_1 = x_2 = 3$. Recalling the choice to divide the domain along the edge $x_1 = x_2$, error in this vicinity may be related to the subdomain division and area mapping. In the vicinity of the substantial notch, the contours are indistinguishable. In general, the ILPGSM solution shows excellent agreement with the analytic solution.

The stress concentration factor in the vicinity of the hole was plotted for the circular hole and a hole with an aspect ratio of 10 in Fig. 8. In each case, ILPGSM overestimated the stress concentration, predicting stress concentrations of 3.2, 12.5, and 24 for the aspect ratios of 1, 5, and 10. Deviations from the analytic solution for the stress concentrations obtained by ILPGSM are 7, 14, and 14% for aspect ratios of 1, 5, and 10, respectively. The erroneous stress predictions in this vicinity could be related to insufficient mesh refinement or applying the boundary conditions via the penalty method along the edge $x_1 = 0$.

The J integral, a measure of the strain energy-release rate or work-per-unit fracture surface area, may be computed by

$$\int_{\Gamma} (W n_2 - n_i \sigma_{ij} u_{j,2}) \, \mathrm{d}\Gamma \tag{26}$$

where W is the strain energy density for elastic material and the elastic strain energy density plus the plastic energy dissipation density for elastic–plastic material under proportional loading. For a line crack in an elastic material, the J integral is path-independent and can be related to the mode I stress intensity factor by [4,5]

$$J = K_1 \left(\frac{1 - \nu^2}{E} \right) \tag{27}$$

Therefore, computing the J integral is a critical element of assessing the damage tolerance of a structural member. For an elliptical notch, the J integral is path-independent; however, it is not independent of the beginning and ending points. This is illustrated in Fig. 9. Paths A and B give the same J integral; however, path C is not equivalent. For the present problem, the J integral was analytically evaluated between the two extreme points along the minor axis (paths A and B in Fig. 9) by Livieri [5] and Livieri and Segala [24]. Accordingly, the J integral is analytically given by

$$J = \frac{\sigma_{\text{norm}}^2}{E} \left\{ \frac{2 r_2^4}{c (r_2 - r_1)^2} \left[\frac{c r_1}{r_2^2} + \tan^{-1}\left(\frac{c}{r_1} \right) \right] - 4 \frac{r_2^2 r_1 c}{(r_2 - r_1)^3} \tan^{-1}\left(\frac{c}{r_1} \right) + \frac{r_1 c^4}{(r_2 - r_1)^4} \right\} \tag{28}$$

where r_2 is the major axis, r_1 is the minor axis, and $c = \sqrt{r_2^2 - r_1^2}$.

The J integral was numerically evaluated from the ILPGSM solution by selecting successive paths on which ξ or η are constant. Three paths were selected and averaged to verify path independence. The paths are shown for an aspect ratio of 10 in the (x_1, x_2) domains

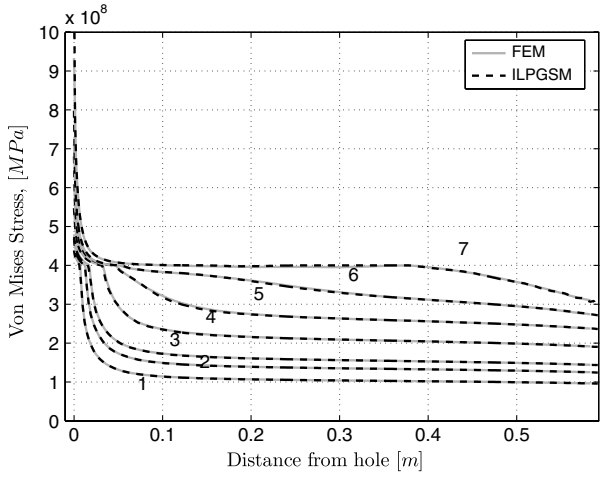

a) Von Mises stress

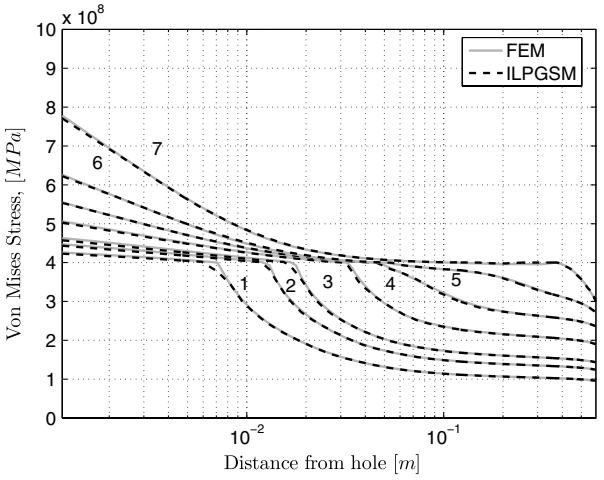

b) Von Mises stress

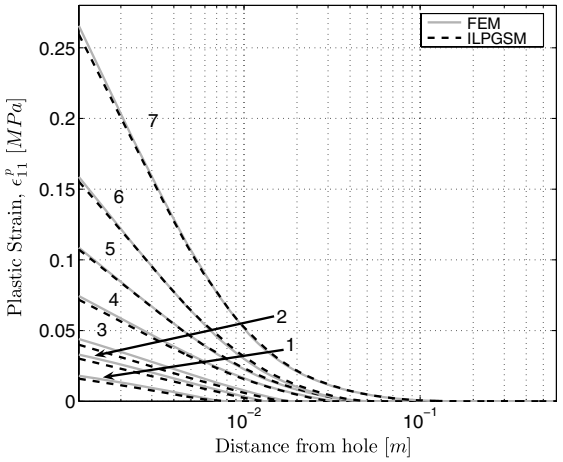

c) Plastic strain

Fig. 17 Von Mises stress and plastic strain for panel with elliptical notch with an aspect ratio of five ($r_2/r_1 = 5$). Load steps 1–100, 2–130, 3–150, 4–200, 5–250, 6–300, and 7–340 MPa.

in Fig. 10. Because of the problem's symmetry, it can be shown that the J integral defined around the whole notch (see Fig. 9) is twice that along the contours shown in Fig. 10. The numerical results were compared with the analytic solution for the increasing aspect ratio in Fig. 11, using $N = 15$. The figure indicates that the J integral compares well with the analytic solution. However, the results deteriorate with the increasing aspect ratio due to increasing severity of the stress concentration. It should be noted that, by increasing the number of sinc points, the accuracy can be recovered for the elliptical cracklike notches.

In Fig. 11, the convergence of the J integral is plotted for increasing the number of sinc points for an aspect ratio of five. The result indicates $N = 15$ (31 sinc points along each axis in each subdomain) provides a converged solution.

IV. Numerical Results for Elastic–Plastic Notched Panel

Elastic–plastic panels with circular and elliptical notches were studied numerically, using the ILPGSM method. The panels were assumed to have a bilinear kinematic hardening material law, as detailed by Kojić and Bathe [25]. The material properties for a generic aluminum alloy were used. The properties are summarized in Table 1.

In each case, the panel had finite dimensions, as shown in Fig. 2, with $a = 0.71$ m and $r_2 = 0.12$ m. Uniform tension was applied to the right edge, and the top surface was free. The symmetry boundary conditions were applied to lines $x_1 = 0$ and $x_2 = 0$ (see Fig. 2). For the panel with a circular notch, the load was increased proportionally from 10 to 340 MPa in steps of 10 MPa. A relative convergence criteria was used to determine convergence of the modified Newton iteration. Convergence was assumed to occur when the norm of the vector of the displacement increment was 1×10^{-4} times the norm of the displacements at the sinc points. That is,

$$\frac{\|\{\Delta u_1(\xi_i, \eta_j), \Delta u_2(\xi_i, \eta_j)\}\|}{\|\{u_1(\xi_i, \eta_j), u_2(\xi_i, \eta_j)\}\|} < 1 \times 10^{-4} \tag{29}$$

where $\{i, j\} = \{-N, -N+1, \ldots, N\}$. The onset of plasticity was estimated to occur at a load of approximately 130 MPa, assuming the panel behaves similarly to the infinite panel.

For a panel with a circular notch, ILPGSM implemented in MATLAB® was used to analyze the problem. The sinc points were distributed using $N = 14$ or $n = 29$ sinc points along each edge in each subdomain and using a mesh size of $2/N$ (see Slemp et al.

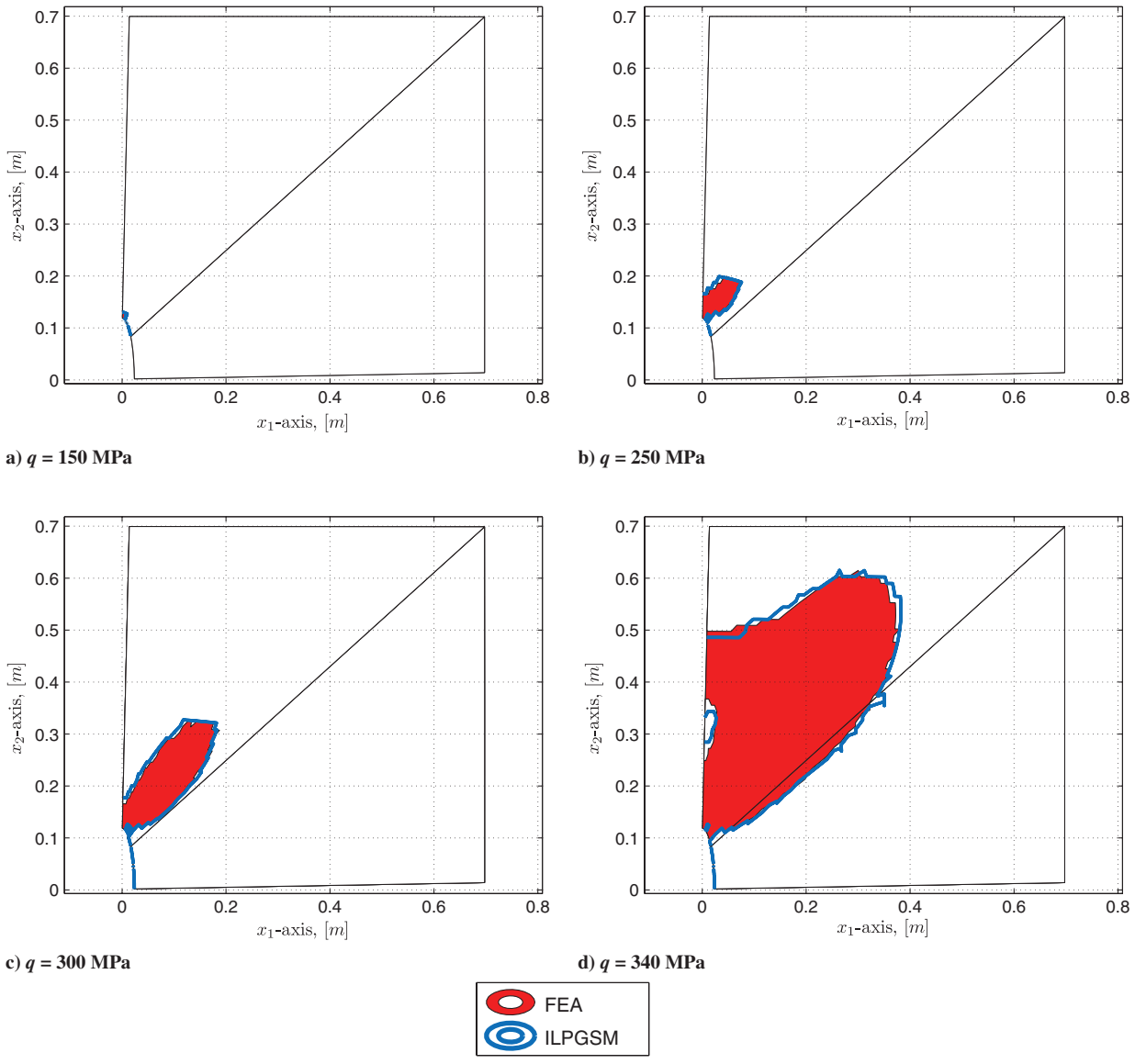

Fig. 18 Growth of plastic zone with increasing applied load by ILPGSM and FEA for elliptical notch with aspect ratio of five ($r_2/r_1 = 5$). The red and blue contours indicate yielded material from the FEA and ILPGSM, respectively.

[13,14]). A total of 1682 sinc points were used, resulting in a system of 4356 equations in 3844 unknowns. For this problem, the QR decomposition using the linear algebra package (LAPACK) took a total of 45 s on a single 2.99 GHz processor. For the panel with an elliptical notch, more sinc points were used. ILPGSM was implemented in FORTRAN 90. The sinc points were distributed, using $N = 20$ or $n = 41$ sinc points along each edge in each subdomain and using a mesh size of $2/N$ (see Slemp et al. [13,14]). A total of 3362 sinc points were used, resulting in a system of 8100 equations in 7396 unknowns. For this problem, the QR decomposition using LAPACK took a total of 297 s on the same 2.99 GHz processor.

Results were compared with a finite-element solution obtained in Abaqus/Standard. For the FEA solution, substantial mesh refinement was performed until a similar solution was obtained by two successively fine meshes. A total of 7163 nodes was used to mesh the panel with a circular hole, and 18,031 nodes were used to mesh the panel with an elliptical hole with an aspect ratio of five. The von Mises stress was examined to insure that there were no stress peaks occurring in only one element. The FEA mesh with boundary conditions and the ILPGSM sinc point distribution may be seen in Fig. 12.

A. Circular Notch

The u_1 displacement of the point $(a, 0)$ (maximum u_1 displacement) was plotted against the applied tension load in Fig. 13. The FEA and ILPGSM solutions are indistinguishable. Note that, while the onset of plasticity occurs near the 130 MPa applied load, the displacement shows very mild nonlinearity until, approximately, the 300 MPa applied load. Near 340 MPa, the panel becomes fully plastic. The von Mises stress and plastic strain (ϵ^p_{11}) were plotted along the line $x_1 = 0$ in Fig. 14 for load increments of $q = 100$, 130, 150, 200, 250, 300, and 340 MPa. The success of the ILPGSM to capture the plasticity is apparent. Note that the ILPGSM performs exceptionally well at capturing the plastic zone size, and tip stress results tend to deteriorate. As the plasticity grows, the stress slope discontinuity moves into areas of less densely populated sinc points (see Fig. 12). This results in deterioration of the results, as evident by slight wiggles in the stress in load steps 6 and 7 and in the drop in plastic strain near the hole in steps 6 and 7.

The growth of the plastic zone size was plotted in Fig. 15. Note that the two analyses provide similar results. In general, ILPGSM results in a larger plastic zone size than the FEA. Note, however, in Fig. 15d, there are additional blue contours, indicating yielded material. This result is likely because of an insufficient refinement in the sinc point distribution and would likely be resolved by increasing the number of sinc points.

B. Elliptical Notch

The u_1 displacement of the point $(a, 0)$ (maximum u_1 displacement) was plotted against the applied tension load in Fig. 16 for a panel with an elliptical notch with an aspect ratio of five. The FEA and ILPGSM solutions are indistinguishable. For the elliptical case, the onset of plasticity occurs near a 36 MPa applied load; however, the plasticity remains localized until, approximately, a 300 MPa applied load. Note that the fully plastic yielding occurs at a load very near the load at which the circular notched panel becomes fully plastic.

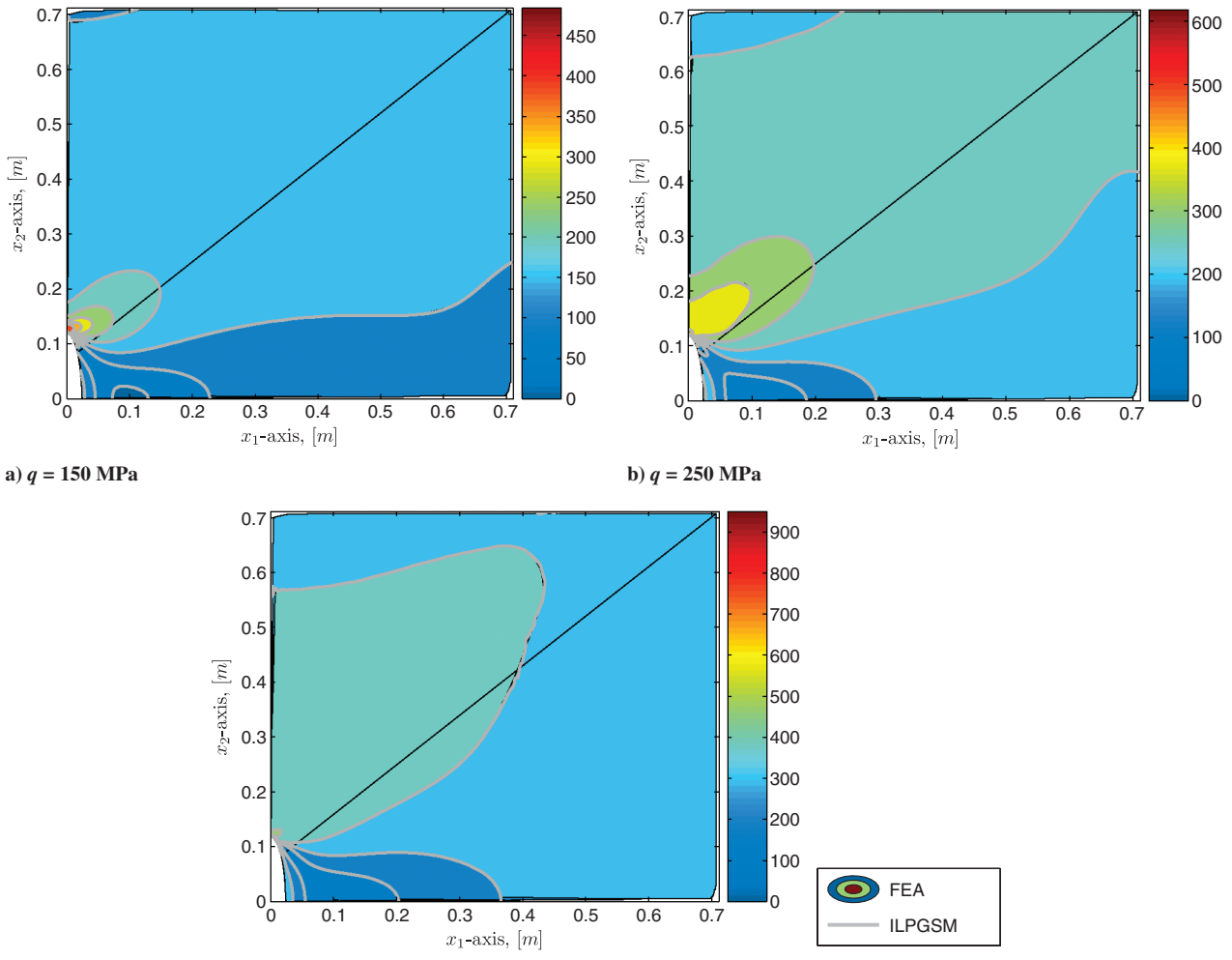

a) q = 150 MPa **b) q = 250 MPa**

c) q = 340 MPa

Fig. 19 Comparison of contours of von Mises stress by ILPGSM and FEA for panel with elliptical hole.

The von Mises stress and the plastic strain are plotted in Fig. 17. The ILPGSM solution and the FEA solution are nearly indistinguishable. Even plotting with a logarithmic ordinance scale, the FEA and ILPGSM solution appear nearly indistinguishable. The plastic strain is predicted slightly higher by the ILPGSM in the direct vicinity of the hole. Nonetheless, the figure indicates an excellent correlation between the ILPGSM and the FEA solutions.

The growth of the plastic zone size was plotted in Fig. 18. The two analyses provide very similar results. The plastic zone size is predicted to be larger in some areas and smaller in others.

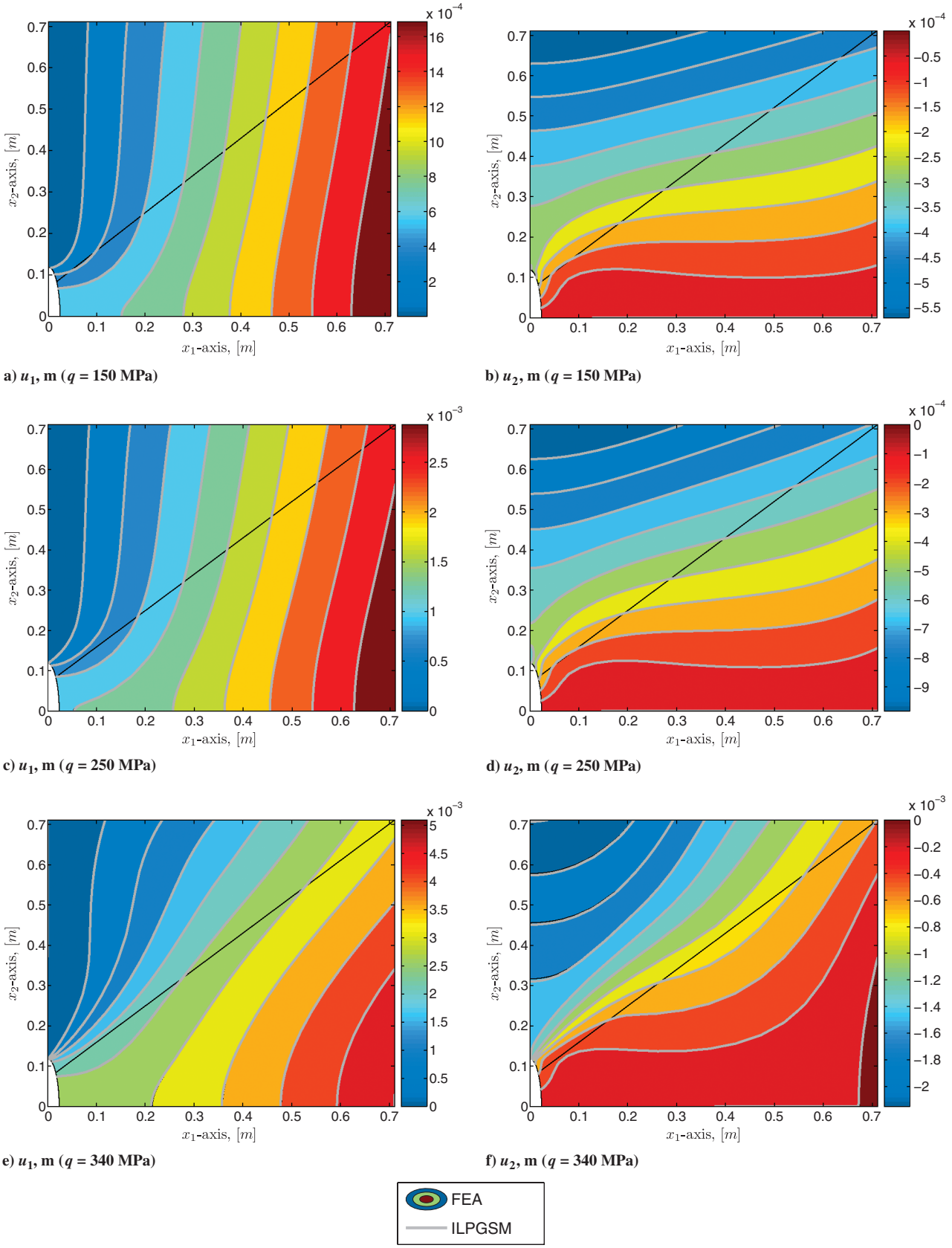

a) u_1, m (q = 150 MPa)

b) u_2, m (q = 150 MPa)

c) u_1, m (q = 250 MPa)

d) u_2, m (q = 250 MPa)

e) u_1, m (q = 340 MPa)

f) u_2, m (q = 340 MPa)

Fig. 20 Comparison of contours of u_1 and u_2 by ILPGSM and FEA for panel with elliptical hole.

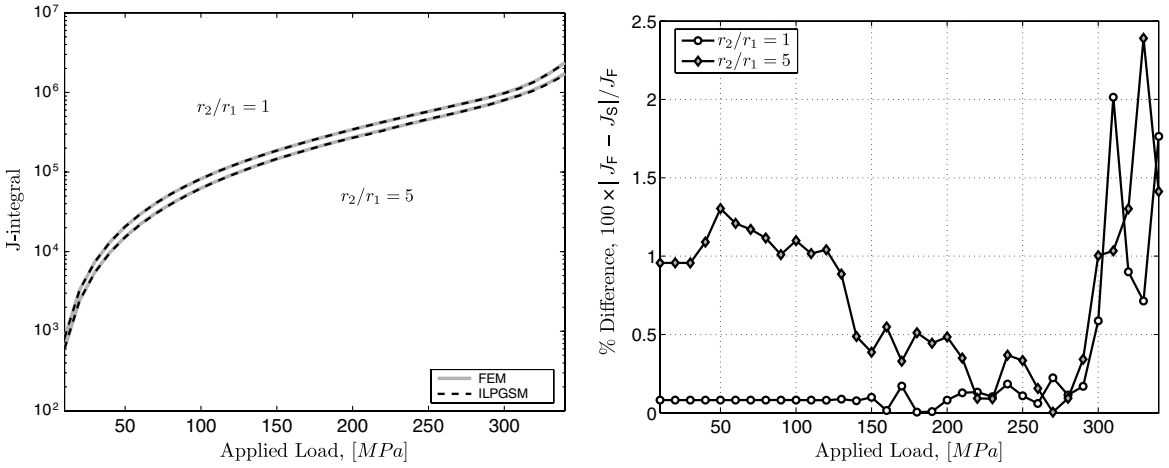

a) J integral **b) % Difference**

Fig. 21 Comparison of *J* integral computed by ILPGSM and Abaqus FEA. *J* integral given in units of N/m.

Furthermore, the figure indicates that there is yielding in the very vicinity of the hole. In this case, the ILPGSM appears to be inaccurate at the boundary of the hole; however, throughout the majority of the domain, the solution shows excellent correlation with the FEA results.

Contours of the von Mises stress for the panel with an elliptical notch were plotted in Fig. 19. Contours of the displacements were plotted in Fig. 20. In each case, the contours are indistinguishable from the FEA result.

C. *J* Integral

The *J* integral was computed for both the panel with a circular hole and an elliptical hole. Abaqus provided a mechanism to compute the *J* integral. For the ILPGSM results, the integral was averaged over the three contours shown in Fig. 10. Five contours were averaged for the FEA results in Abaqus. The results are compared in Fig. 21. The *J* integral is computed within 2 and 2.5% of the FEA for the circular and elliptic holes, respectively.

V. Conclusions

In this paper, the ILPGSM was extended for analysis of elastic–plastic materials. Both elastic and elastic–plastic plane-stress panels with elliptical and circular notches were considered. The physical domain was decomposed into two subdomains that were transformed onto square domains in the fashion of isoparametric finite elements. The essential boundary conditions and the continuity between subdomains were imposed by the traditional penalty method. The results show the ILPGSM provides sufficient accuracy for both elastic and elastic–plastic problems. While the approach implemented could handle any loading and unloading, only proportional loading was considered, and the *J* integral was computed using three contours. The elastic panel was compared with the analytic solution for the problem [23]. The elastic–plastic problem was compared with a FEA performed in Abaqus. The results indicates a high level of accuracy for both the linear and nonlinear problems, even with large levels of plastic flow occurring. The accuracy decreases for an increasing hole aspect ratio (with the same number of sinc points), a result which is not surprising because, with a finite-element solution, more elements are required for a converged solution for the highly elliptic, cracklike notch.

Acknowledgments

We would like to thank the U.S. Department of Defense and the U.S. Army Research Office for funding the National Defense Science and Engineering Graduate Fellowship that supported this work in part. We would also like to thank NASA Langley Research Center for facilities and support of this and other projects. We extend our sincere gratitude to Kim S. Bey and R. Keith Bird of NASA Langley Research Center for conversations regarding the present implementation. Furthermore, we extend our gratitude to the two reviewers whose comments were very constructive in developing this manuscript.

References

[1] Newman, J. C., James, M. A., and Zerbst, U., "A Review of the CTOA/CTOD Fracture Criterion," *Engineering Fracture Mechanics*, Vol. 70, Nos. 3–4, 2003, pp. 371–385. doi:10.1016/S0013-7944(02)00125-X

[2] Rice, J. R., "A Path Independent Integral and the Approximate Analysis of Strain Concentration by Notches and Cracks," *Journal of Applied Mechanics*, Vol. 35, 1968, pp. 379–386.

[3] Dowling, N. E., *Mechanical Behavior of Materials*, 3rd ed., Prentice–Hall, Upper Saddle River, NJ, 2007.

[4] Livieri, P., "A New Path Independent Integral Applied to Notched Components under Mode-I Loadings," *International Journal of Fracture*, Vol. 123, No. 3, Oct. 2003, pp. 107–125. doi:10.1023/B:FRAC.0000007371.25227.aa

[5] Livieri, P., "Use of *J*-Integral to Predict Static Failures in Sharp V-Notches and Rounded U-Notches," *Engineering Fracture Mechanics*, Vol. 75, No. 7, May 2008, pp. 1779–1793. doi:10.1016/j.engfracmech.2007.01.022

[6] Berto, F., and Lazzarin, P., "Relationships Between *J*-Integral and the Strain Energy Evaluated in a Finite Volume Surrounding the Tip of Sharp and Blunt V-Notches," *International Journal of Solids and Structures*, Vol. 44, Nos. 14–15, July 2007, pp. 4621–4645. doi:10.1016/j.ijsolstr.2006.11.041

[7] Faleskog, J., and Nordlund, P., "Near-Tip Field Characterization and *J*-Integral Evaluation for Nonproportional Loads," *International Journal of Solids and Structures*, Vol. 31, No. 1, 1994, pp. 1–26. doi:10.1016/0020-7683(94)90172-4

[8] Blackburn, W., "Path Independent Integrals to Predict Onset of Crack Instability in an Elastic Plastic Material," *International Journal of Fracture*, Vol. 8, No. 3, Sept. 1972, pp. 343–346. doi:10.1007/BF00186134

[9] Simha, N., Fischer, F., Shan, G., Chen, C., and Kolednik, O., "*J*-Integral and Crack Driving Force in Elastic–Plastic Materials," *Journal of the Mechanics and Physics of Solids*, Vol. 56, No. 9, 2008, pp. 2876–2895. doi:10.1016/j.jmps.2008.04.003

[10] Gu, Y., Wang, Q., Lam, K., and Dai, K., "A Pseudo-Elastic Local Meshless Method for Analysis of Material Nonlinear Problems in Solids," *Engineering Analysis with Boundary Elements*, Vol. 31, No. 9, 2007, pp. 771–782. doi:10.1016/j.enganabound.2006.12.008

[11] Ma, J., Xin, X., and Krishnaswami, P., "Elastoplastic Meshless Integral Method," *Computer Methods in Applied Mechanics and Engineering*, Vol. 197, Nos. 51–52, 2008, pp. 4774–4788. doi:10.1016/j.cma.2008.06.019

[12] Zhang, Y., and Chen, L., "Impact Simulation Using Simplied Meshless Method," *International Journal of Impact Engineering*, Vol. 36, No. 5, 2009, pp. 651–658.

doi:10.1016/j.ijimpeng.2008.11.007
[13] Slemp, W. C. H., Kapania, R. K., and Mulani, S. B., "Integrated Local Petrov–Galerkin Sinc Method for Structural Mechanics Problems," 50th AIAA/ASME/ASCE/AHS/ASC Structures, Structural Dynamics, and Materials Conference (SDM Conference), AIAA Paper 2009-2392, May 2009.
[14] Slemp, W. C. H., Kapania, R. K., and Mulani, S. B., "Integrated Local Petrov–Galerkin Sinc Method for Structural Mechanics Problems," *AIAA Journal*, Vol. 48, No. 6, June 2010, pp. 1141–1155. doi:10.2514/1.45892
[15] Li, C., and Wu, X., "Numerical Solution of Dierential Equations Using Sinc Method Based on the Interpolation of the Highest Derivatives," *Applied Mathematical Modelling*, Vol. 31, No. 1, 2007, pp. 1–9. doi:10.1016/j.apm.2006.04.013
[16] Slemp, W. C. H., and Kapania, R. K., "Imposing Boundary Conditions in Sinc Method Using Highest Derivative Approximation," *Journal of Computational and Applied Mathematics*, Vol. 230, No. 2, Aug. 2009, pp. 371–392. doi:10.1016/j.cam.2008.12.006
[17] Slemp, W. C. H., and Kapania, R. K., "Interlaminar Stresses by Sinc Method Based on Interpolation of the Highest Derivative," *AIAA Journal*, Vol. 46, No. 12, 2008, pp. 3128–3141. doi:10.2514/1.39613
[18] MacLeod, A. J., "Rational Approximations, Software and Test Methods for Sine and Cosine Integrals," *Numerical Algorithms*, Vol. 12, No. 2, 1996, pp. 259–272. doi:10.1007/BF02142806
[19] Reddy, J. N., *An Introduction to the Finite Element Method*, 3rd ed., McGraw–Hill, New York, 2004.
[20] Zhu, T., and Atluri, S. N., "A Modified Collocation Method and a Penalty Formulation for Enforcing the Essential Boundary Conditions in the Element Free Galerkin Method," *Computational Mechanics*, Vol. 21, No. 3, April 1998, pp. 211–222. doi:10.1007/s004660050296
[21] Schaback, R., "Recovery of Functions from Weak Data Using Unsymmetric Meshless Kernel-Based Methods," *Applied Numerical Mathematics*, Vol. 58, No. 5, 2008, pp. 726–741. doi:10.1016/j.apnum.2007.02.009
[22] Batra, R. C., and Zhang, G., "SSPH Basis Functions for Meshless Methods, and Comparison of Solutions with Strong and Weak Formulations," *Computational Mechanics*, Vol. 41, No. 4, March 2008, pp. 527–545. doi:10.1007/s00466-007-0209-3
[23] Muskhelishvili, N. I., *Some Basic Problems of the Mathematical Theory of Elasticity: Fundamental Equations, Plane Theory of Elasticity, Torsion and Bending*, 4th ed., Springer, New York, 1954.
[24] Livieri, P., and Segala, F. "Analytical Evaluation of J-integral for Elliptical and Parabolic Notches Under Mode I and Mode II Loading," *International Journal of Fracture*, Vol. 148, No. 1, 2007, pp. 57–71. doi:10.1007/s10704-008-9178-6
[25] Kojić, M., and Bathe, K.-J., *Inelastic Analysis of Solids and Structures (Computational Fluid and Solid Mechanics)*, 1st ed., Springer, New York, Dec. 2004.

A. Palazotto
Associate Editor